Chapter 5

Beam monitoring: analysis and results

5.1 Overview

With the new high-intensity accelerator beam facilities becoming more and more powerful, while attempting measurements at increasingly high precision, real time beam monitoring is becoming essential, both to protect equipment, and to precisely measure beam properties. The simulations and analysis performed for this thesis aim to evaluate the beam monitoring capabilities of SAND for the DUNE neutrino beam.
Many observables can be used for beam monitoring. In this study we have considered the reconstructed momenta of muons produced in ν_μ CC interactions in SAND's front electro-magnetic calorimeter modules. The shape of the reconstructed momentum spectrum of the muons produced in CC interactions, depends on the original ν_μ energy spectrum. Any anomalies in the beam production would thus in principle cause variations in both spectra. In particular we considered the anomalies generated when the second neutrino beam horn experienced a transverse displacement of +0.5 mm in the Y coordinate
The nominal and modified interactions samples were simulated using the GENIE neutrino Montecarlo generator to have vertex in one of the nine frontal barrel calorimeter modules (Figure 5.1). The particles produced in the interactions were then propagated with edep-sim, the ECAL and STT signals were digitized and the clusters and tracks reconstructed. Note that in order to shorten the simulation times the digitization and reconstruction steps were performed only on the primary particles of the interactions.
No particle identification has been implemented for SAND's simulation chain at the time of writing. The muon tracks where thus selected post reconstruction from

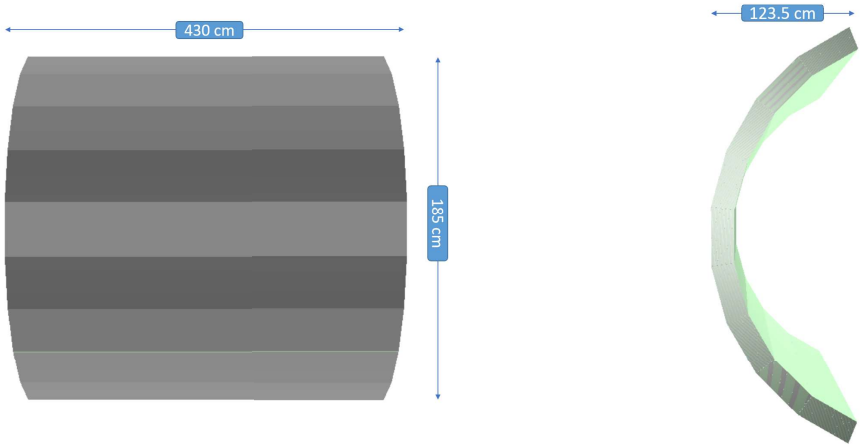

(a) (b)

Figure 5.1: Graphical representation (produced with OGL) of the 9 front calorimeter barrel modules GEANT4 geometries. The two panels show the projection (a) on the xy plane and (b) on the yz plane.

the Montecarlo truth PDG code informations. In order to select only the muons produced in CC interactions in the inner layers of the calorimeter, a selection on the energy deposition on the most outer layer of the ECAL was implemented. This energy deposition threshold, together with a selection on the x position of the neutrino vertexes defined our fiducial cut.
Only the successfully reconstructed muons were considered. Additionally the χ^2 values for the linear and circular fits were used to identify a reconstruction quality selection.
We studied the sensitivity to the beam modification by applying two-sample homogeneity tests on the reconstructed muon momentum distributions. We used samples roughly corresponding to the amount of CC interactions expected in the front calorimeters of SAND in a week, as suggested by the ND collaboration for beam monitoring measures. Given the CC interaction event rate $r_{CC} = 4.685 \times 10^5$ ev$[\nu_\mu(CC)]$/ton/week, the module mass $m_{mod} = 2.75$ ton, the number of target modules $n_{mod} = 9$ and the fraction of CC events with respects to the total $f_{CC} = 2/3$ this corresponds to:

$$N_{week} = r_{CC} \times f_{CC}^{-1} \times m_{mod} \times n_{mod} \simeq 1.74 \times 10^6 \tag{5.1}$$

We thus produced a "nominal" (standard neutrino beam energy distribution) and a "shifted" (neutrino beam produced with +0.5 mm Y shift in the second horn) sample both containing exactly $N = 1750000$ neutrino interactions.

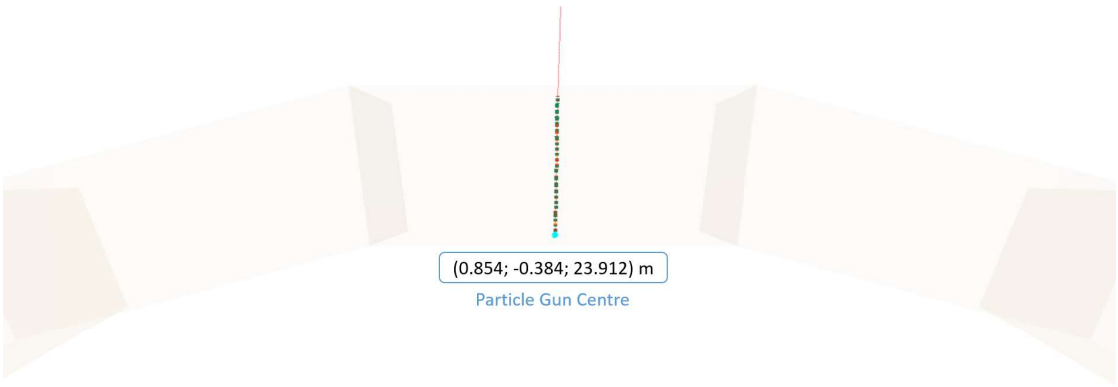

Figure 5.2: A 10 GeV up-going muon hitting SAND's top calorimeter module, simulated using the edep-sim GEANT4 particle gun option and drawn using edep-disp. The red line indicates the muon track, with the hits inside the calorimeter being individually highlighted. The particle gun centre is shown as a light-blue dot together with its (x, y, z) ND hall coordinates.

5.2 Preliminary measurements

A series of preliminary measurements were needed before the application of the beam monitoring tests. Firstly we needed to extrapolate the calibration coefficient between the energy loss of a minimum ionizing particle (MIP) in a calorimeter module cell and the total number of p.e. produced. This was essential to be able to set the p.e. threshold used for the outer layer cut.
An evaluation of the reconstruction algorithm efficiency with respect to energy was also performed, together with a study on the efficiency of the front layer energy deposition cut and reconstruction selection.

5.2.1 Muon energy loss calibration

In order to measure the calibration constant between the MIP loss and the photo-electron production in the calorimeter cells, we simulated a set of 1000 up-going muons with an initial energy of 10 GeV, hitting the top calorimeter barrel module's inner base at the centre of one of its cells. The muons were generated using a simple GEANT4 particle gun via edep-sim, while the geometry is the same as for the general simulation. A graphical representation of one of these events is shown in Figure 5.2. The particle gun was placed on the surface of the calorimeter so that no interactions with other elements of the geometry were possible before the particle hit the module.
The hits and relative energy losses were then assigned to the calorimeter cells during digitization producing two ADC values for each cell. The distribution

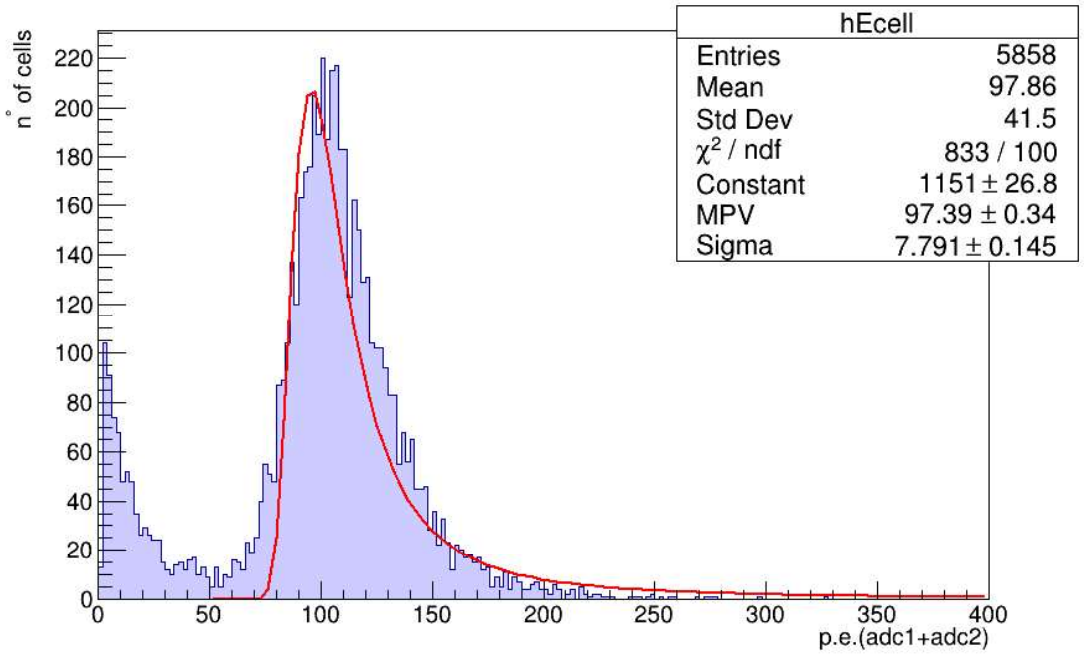

Figure 5.3: Distribution of total number of photo-electrons produced at the passage of a 10 GeV muon in a ECAL cell. The histogram has been produced from a set of 1000 simulated muons hitting a calorimeter module. These were generated using the GEANT4 particle gun mode implemented in edep-sim. The red line indicates a Landau fit, the results of which are summarized in the box in the upper right corner of the histogram canvas.

of the sum of the two ADC values, which in our simple digitization algorithm corresponds with the total production of photo-electrons, is shown in Figure 5.3. Performing a Landau fit on the histogram we find that the most probable value is:

$$N_{p.e.}^{cell} = (97.39 \pm 0.34) \text{ p.e.} \tag{5.2}$$

We can approximate the energy loss of the muon with the one experienced by a minimum ionizing particle (MIP) traversing 40 slabs of lead for a total of $\Delta x_{Pb} = 1.6$ cm and 40 slabs of plastic scintillator for a total thickness of $\Delta x_{Sc} = 2.8$ cm:

$$\Delta E_{cell} \simeq \left(\frac{dE}{dx}\right)^{MIP} \rho_{Pb} \Delta x_{Pb} + \left(\frac{dE}{dx}\right)^{MIP} \rho_{Sc} \Delta x_{Sc} \simeq 42.22 \text{ MeV} \tag{5.3}$$

where $(dE/dx)^{MIP} \sim 2$ MeV/(g/cm^2) is the average energy loss of a MIP and $\rho_{Pb} = 11.34$ g/cm^3 and $\rho_{Sc} = 1.06$ g/cm^3 are the densities of lead and the scintillating material respectively.

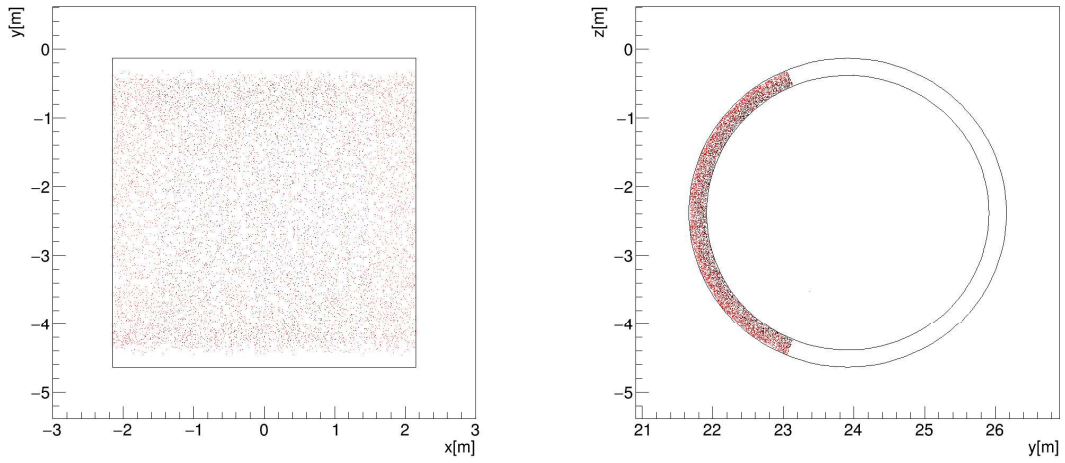

(a) (b)

Figure 5.4: Spatial distribution in ND hall global coordinates of the true neutrino interaction vertexes of the events that survive the outer layer cut (black) and those that don't (red). The two panels show the projection (a) on the xy plane and (b) on the yz plane. A simplified profile of the ECAL barrel is outlined in black.

The average number of photo-electrons produced per cell per MeV is given by the calibration coefficient:

$$c = \frac{N_{p.e.}^{cell}}{\Delta E_{cell}} \simeq 2.31 \text{ [p.e./Mev]} \tag{5.4}$$

This is roughly in agreement with previous calibrations performed by the KLOE collaboration using cosmic ray muons, which measured an average number of p.e. per PMT per MeV of about 1 p.e./MeV [69].

5.2.2 Fiducial cut

Selecting from the total one week nominal sample of 1.75×10^6 events, only the ν_μ CC interactions, we are left with 1318845 events. All the muons in this sample are the product of CC interactions in the front calorimeter modules. In a realistic physical scenario, the sample would include also a certain amount of muons that are the product of ν_μ CC from outside the detector either from the neutrino beam or from cosmic rays.
In order to eliminate these external events from our sample we introduce an energy deposition threshold on the outer layer of $\Delta E_{th} = 15$ MeV. Using the calibration coefficient found in Section 5.2.1 we then find the threshold in number of total

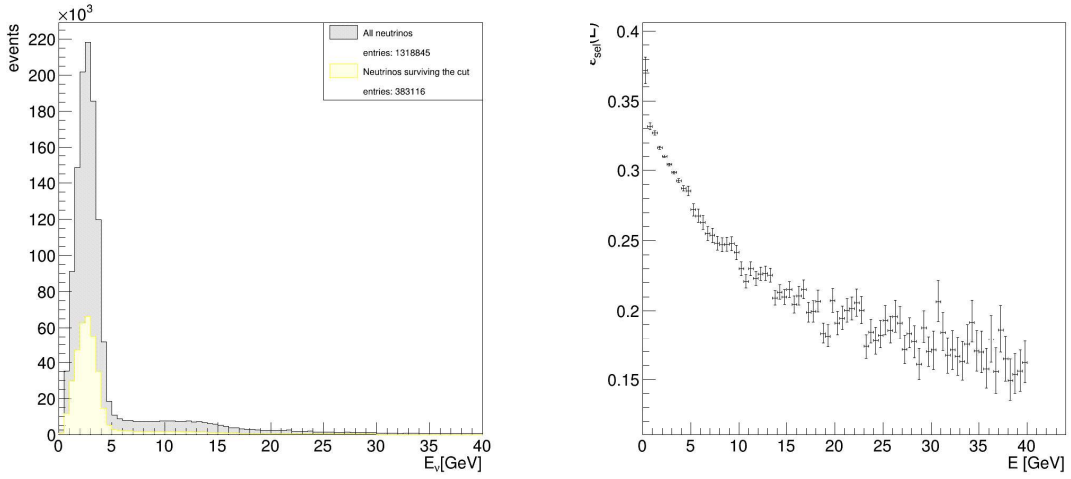

(a) (b)

Figure 5.5: (a) Energy (Montecarlo truth) distribution of neutrinos from the CC nominal sample (grey); Energy (Montecarlo truth) distribution of neutrinos surviving the fiducial cut (yellow) (b) Selection efficiency as a function of neutrino energy from the Montecarlo truth.

photo-electrons produced:

$$N_{p.e.}^{th} = c \times \Delta E_{th} \simeq 35 \text{ p.e.} \tag{5.5}$$

Any event having photo-electron production on the outer layer ≥ 35 p.e. is discarded.

In order to eliminate the events that are likely going to produce muons that won't fully traverse the STT, which we expect to have poor momentum reconstruction, we also define a spatial cut on the x position of the interaction vertex:

$$|x_V| \leq 1.5 \text{ m} \tag{5.6}$$

In order to estimate the vertex position we use the space information from the front calorimeter modules' cells in which there has been an energy deposition. Specifically we evaluate x_V as a weighted average on the ADC deposits E_i^{cell}:

$$x_V = \frac{\sum_{i=1}^{N_{cell}} x_i^{cell} E_i^{cell}}{E_{tot}^{cell}} \tag{5.7}$$

N_{cell} is the number of hit cells, x_i^{cell} is the estimated position of the particle transit within the cell and E_{tot}^{cell} is the total ADC p.e. production in the front calorimeter

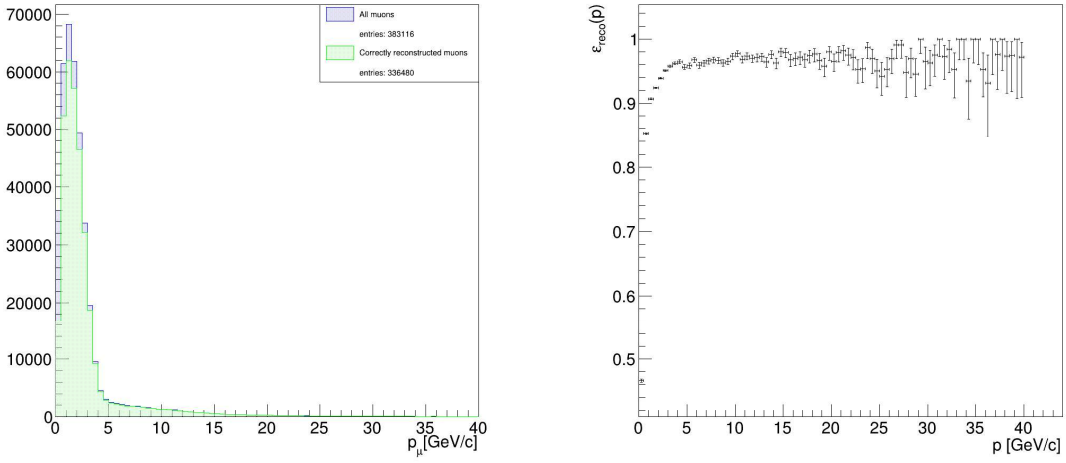

(a) (b)

Figure 5.6: (a) Distributions of the true Montecarlo momenta of the muons from the fiducial sample (blue) and only the ones correctly reconstructed (green) (b) Reconstruction algorithm efficiency as a function of the true Montecarlo muon momentum.

modules.
We define the combination of the outer layer energy deposition and the vertex selection as our fiducial cut. In Figure 5.4 we show the spatial distribution of the interaction vertexes of the events surviving the fiducial cut (black), together with those that don't (red). In Figure 5.5 (a) we show the distribution of the true Montecarlo neutrino energy before and after the cut.
We can define the cut efficiency ε_{cut} as the ratio between the events surviving the selection $N_{fid} = 383116$ and the total number of CC events $N_{CC} = 1318845$:

$$\varepsilon_{cut} = \frac{N_{fid}}{N_{CC}} = 0.2905 \pm 0.0005 \tag{5.8}$$

The selection efficiency distribution with respects to the neutrino energy is shown in Figure 5.5 (b). Note that ε_{cut} gets worse at higher energy. This is might be due to nuclei fragmentation in DIS ν_μ interactions which produce a large quantity of scattered nucleons that can deposit energy in the calorimeter.

5.2.3 Muon track reconstruction efficiency

The STT track reconstruction algorithms described in Section 4.5 can sometimes fail. If either one of the two fits fail, the reconstruction is considered unsuc-

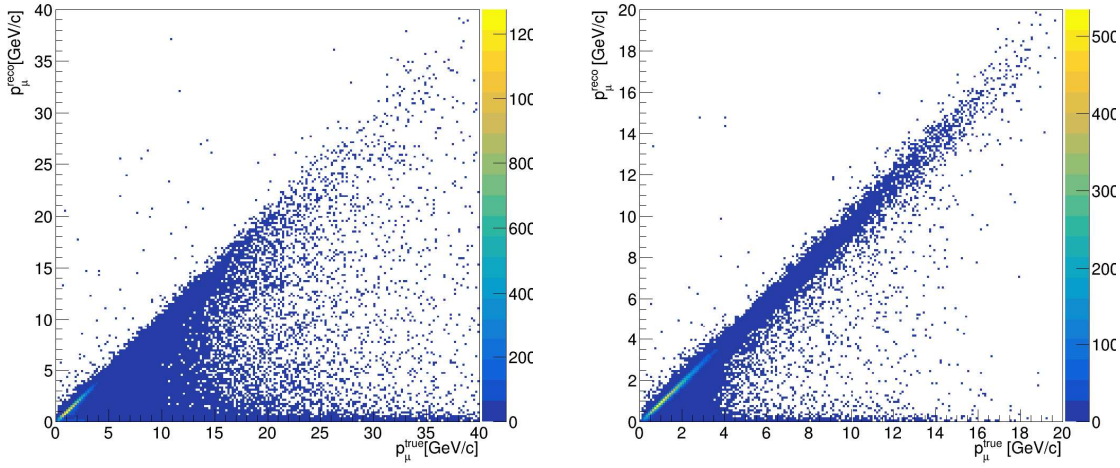

(a) (b)

Figure 5.7: Reconstructed momenta as a function of the true Montecarlo ones, before (a) and after (b) the quality cut is applied

cessful and the event is flagged and discarded for the final momentum reconstruction.
The circular fit is considered not successful if the track has less than three hits on horizontal straw tubes. The linear fit always fails if the circular fit is unsuccessful, since it necessitates the (y_C, z_C) and R estimates in order to calculate the ρ coordinates. The other failure conditions are analogous to the circular fit ones, with additional problems occurring when extrapolating the y coordinate from the x and z values obtained from the vertical straws.
The total reconstruction efficiency is given by the ratio between the number of correctly reconstructed muons $N_{reco} = 351267$ and the total number of muons in the fiducial sample $N_{fid} = 400329$:

$$\varepsilon_{reco} = \frac{N_{reco}}{N_{fid}} = 0.878 \pm 0.002 \tag{5.9}$$

In Figure 5.6 (a) we show the distribution of the muon real momenta from the two samples and in Figure 5.6 (b) we show ε_{reco} as a function of the muon momentum.

5.2.4 Quality selection

By plotting the reconstructed muon momentum of those events for which the track fits were considered successful (Figure 5.7 (a)), we see that in a considerable amount of cases, especially at low energies, p_μ is underestimated. We might then

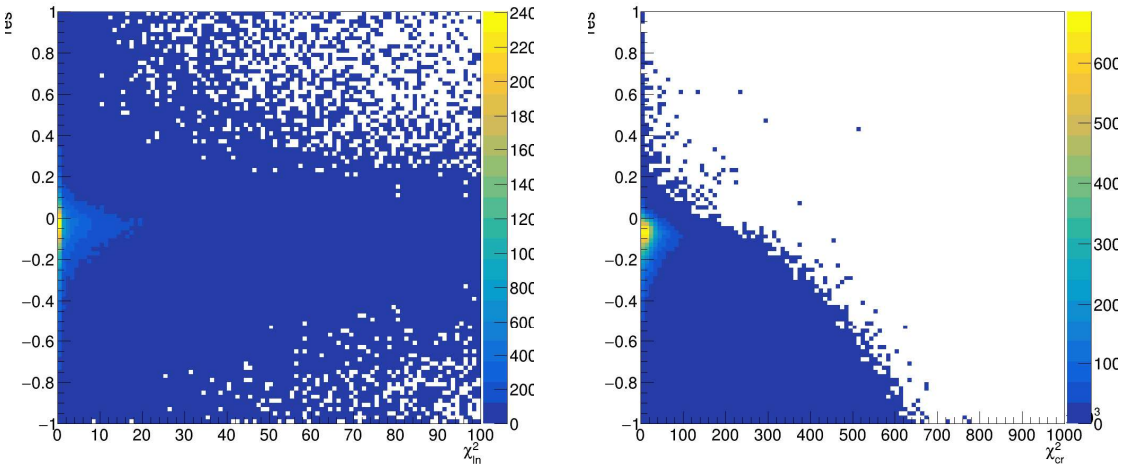

(a) (b)

Figure 5.8: (a) χ^2_{ln} as a function res; (b) χ^2_{cr} as a function of res. The fiducial cut and reconstruction successfulness cuts have both been applied to the samples.

want to calculate χ^2-like statistic values for linear (χ^2_{ln}) and circular (χ^2_{cr}) fits and use them to select a sample of well reconstructed muons. For the linear fit (see Section 4.5.2 for the definitions of the variables) performed on N_{hits} straw hits we define:

$$\chi^2_{ln} = \frac{1}{N_{hits}} \sum_{i=1}^{N_{hits}} (x_i - x_0 - \rho_i \tan\lambda)^2 \tag{5.10}$$

and for the circular fit:

$$\chi^2_{cr} = \frac{1}{N_{hits}} \sum_{i=1}^{N_{hits}} |(y_i - y_C)^2 + (z_i - z_C)^2 - R^2| \tag{5.11}$$

We try to gauge what such a cut might be by plotting the χ^2 of the linear and circular fits as a function of momentum resolution:

$$res = 1 - p_\mu^{true}/p_\mu^{reco} \tag{5.12}$$

The plots are shown in Figure 5.8 (a) and (b) respectively. Starting from these resolution distributions and proceeding by trial and error we found the selection:

$$\chi^2_{ln} < 10^5 \tag{5.13}$$

In Figure 5.7 (b) we show the reconstructed momenta as a function of the true Montecarlo momenta after the quality cut is applied. The efficiency of this selection

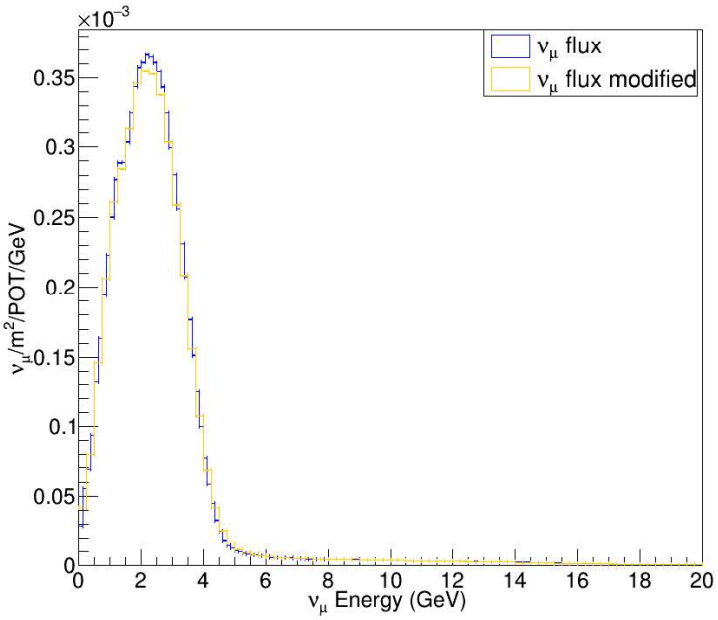

Figure 5.9: (Blue) Muon neutrino flux as a function of neutrino energy produced by the DUNE neutrino beam in standard conditions (Orange) Muon neutrino flux as a function of neutrino energy generated when the second horn had a transverse displacement of +0.5 mm in the Y coordinate.

is given by the ratio between the number of events having sufficiently small χ^2 values $N_{qual} = 326322$ and the total amount of reconstructed muons N_{reco}:

$$\varepsilon_{qual} = \frac{N_{qual}}{N_{reco}} = 0.970 \pm 0.002 \tag{5.14}$$

5.3 Beam monitoring study results

To perform the beam monitoring measurements, we considered the muon neutrino flux produced by the neutrino beam in standard conditions and we confronted it with the one generated when the second horn had a transverse displacement of +0.5mm in the Y coordinate. The corresponding neutrino fluxes simulated by the Beam facilities group as a function of energy in units of $\nu_\mu/m^2/POT/\text{GeV}$ are shown in Figure 5.9.
Note that the ν_μ fluxes were also generated by the collaboration with modifications to many other critical parameters. These include: transverse displacement in both horns and the proton beam; modifications in the proton beam radius and angle on target; shifts in the values of the decay pipe radius, horn currents, target density

and horn water layer thickness. The critical parameter for this study has been selected arbitrarily and is not of special interest over any of the others.

5.3.1 Two-sample statistical tests

In order to spot an anomaly in the neutrino beam production, we would like to test if the modified muon energy spectrum is not consistent with the original one i.e. if the hypothesis that the two histograms are sampled from the same distributions is incorrect. We do not have a clearly defined null hypothesis for what the common distribution would be, so we can only compare the two histograms bin by bin with a so called two-sample statistical test [70]. Of the many possible tests that exist we decided to use three: the χ^2 test, which is a valid two-sample test in the large sample approximation; the Kolmogorov-Smirnov test; the Anderson-Darling test. We implemented the first as a C++ algorithm, while for the second and third we used the ROOT functions KolmogorovTest and AndersonDarlingTest [71]. Since the χ^2 test is the only one directly implemented by me, the p-values obtained with it will be treated as the reference.

Two-sample χ^2 test

Given two histograms with the same number of bins k and boundaries, the bin contents are the realisations of two random variables U and V. We call u_i and v_i the real bin contents and μ_i and ν_i their expected values. The bin contents distributions have the shapes of Poisson functions and the sampling distributions of the difference between the two histograms is:

$$P(\Delta_i) = \frac{1}{(2\pi)^{k/2}} \left(\prod_{i=1}^{k} \frac{1}{\sigma_i} \right) \exp\left(-\frac{1}{2} \sum_{i=1}^{k} \frac{\Delta_i^2}{\sigma_i^2} \right) \tag{5.15}$$

where $\Delta_i = u_i - v_i$ is the difference between the bin contents and σ_i is its standard deviation. We may now construct the test statistic:

$$T = \sum_{i=1}^{k} \frac{(\Delta_i)^2}{\sigma_i^2} \tag{5.16}$$

Considering that the mean of the Poisson distribution coincides with its variance, we can estimate sigma as:

$$\hat{\sigma}_i^2 = (u_i + v_i) \tag{5.17}$$

The test statistic then finally becomes:

$$T = \sum_{i=1}^{k} \frac{(u_i - v_i)^2}{u_i + v_i} \tag{5.18}$$

Note that if for bin i we have $u_i = v_i = 0$, its contribution to the sum is zero.
T follows approximately a χ^2 distribution for $k-1$ degrees of freedom, as long as we are in a situation where the two samples are large enough that the bin contents are distributed normally. We can thus estimate from the χ^2 distribution, the p-value, which in this case is the probability of having two histograms that are as in agreement or less than the ones we are testing, if they are sampled from the same distribution.

Kolmogorov-Smirnov test

The two-sample Kolmogorov-Smirnov test consists in measuring the maximum difference between the two cumulative distribution functions (CDFs) and compare with the null homogeneity hypothesis expectations.
We approximate the cumulative distribution functions as histograms:

$$u_{ci} = \sum_{j=1}^{i} u_j / N_u \tag{5.19}$$

$$v_{ci} = \sum_{j=1}^{i} v_j / N_v \tag{5.20}$$

The test statistic is then given by:

$$T_{KS} = \max_i |u_{ci} - v_{ci}| \tag{5.21}$$

The null hypothesis is rejected at significance level α if:

$$T_{KS} \geq c(\alpha) \sqrt{\frac{N_u + N_v}{N_u \cdot N_v}} \tag{5.22}$$

where $c(\alpha)$ is the inverse of the Kolmogorov distribution and in general can be calculated approximately as:

$$c(\alpha) = \sqrt{-\ln(\alpha/2) \cdot (1/2)} \tag{5.23}$$

Note that the Kolmogorov-Smirnoff test tends to emphasize differences near the peak of the distribution, where the largest fluctuations are expected for Poisson probabilities.

The Anderson-Darling test

The Anderson-Darling test is a modified version of the Kolmogorov-Smirnov test design to improve the sensitivity to the tails of the CDFs. The original statistical test, designed to test the compatibility of a data set x having an empirical CDF $F_m(x)$, with a continuous distribution, having the CDF $F_0(x)$ under the null hypothesis is:

$$A_m^2 = m \int_{-\inf}^{\inf} \frac{[F_m(x) - F_0(x)]^2}{F_0(x)[1 - F_0(x)]} dF_0(x) \tag{5.24}$$

Scholz and Stephens adapted this statistic to the k-sample case, which in our simple two-sample situation reads:

$$T_{AD} = \frac{1}{N_u + N_v} \sum_{j=k_{min}}^{k_{max}-1} \frac{u_j + v_j}{\Sigma_j (N_u + N_v - \Sigma_j)} \times \left[((N_u + N_v)\Sigma_{uj} - N_u \Sigma_j)^2 / N_u + ((N_u + N_v)\Sigma_{vj} - N_v \Sigma_j)^2 / N_v \right] \tag{5.25}$$

where k_{min} is the first non-zero bin for both histograms, k_{max} is the number of bins until the last non-zero bin and:

$$\Sigma_{uj} = \sum_{i=1}^{j} u_i; \quad \Sigma_{uj} = \sum_{i=1}^{j} u_i; \tag{5.26}$$

$$\Sigma_j = \sum_{i=1}^{j} (u_i + v_i) = \Sigma_{uj} + \Sigma_{vj} \tag{5.27}$$

The null hypothesys can be rejected at α confidence level for a test if:

$$\frac{T_{AD} - 1}{\sigma_{(N_u+N_v)}} \geq z_2(1 - \alpha) \tag{5.28}$$

where $z_2(1 - \alpha)$ is the $(1 - \alpha)$-percentile of the standardized asymptotic function $Z_{k-1} = [T_{AD} - 1]/\sigma_{(N_u+N_v)}$ and σ_N is the standard deviation of T_{AD}. More information on how these parameters are defined and on how ROOT implements the Anderson-Darling test can be found in [72].

5.3.2 The control samples

As a first control on our methodology we decided to apply the χ^2 test to the reconstructed momenta from two nominal samples. If the method is capable of distinguishing between the products of two different neutrino beam configurations, we expect to obtain a p-value for two control samples that follow the same distribution that is close to 1. We derive the two samples by applying the fiducial cut

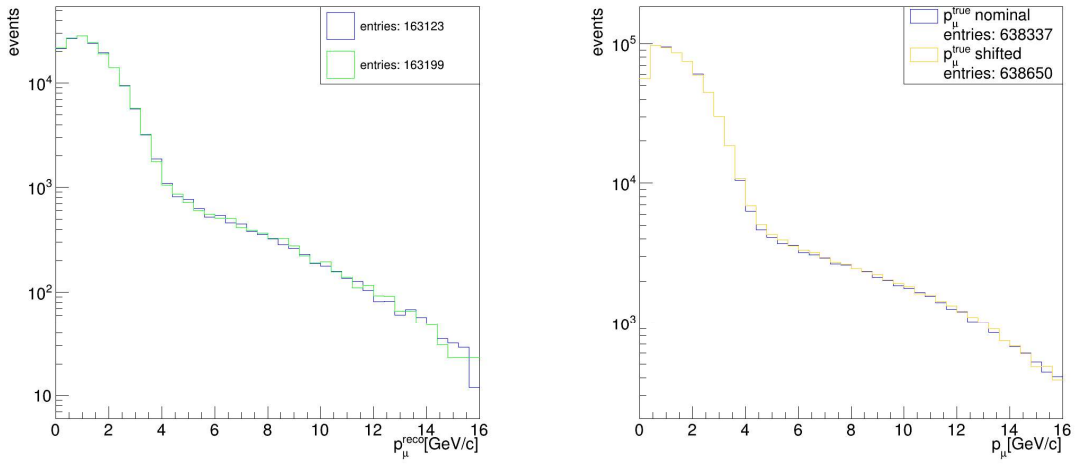

(a) (b)

Figure 5.10: (a) Reconstructed momenta distributions from two control half-statistics samples produced with the nominal neutrino beam. The fiducial and momentum reconstruction successfulness cuts are applied (b) True Montecarlo momenta distributions from the nominal and shifted samples. A fiducial cut is applied. Both histograms are in logarithmic scale.

and momentum reconstruction control to the one week simulation and dividing the events randomly into two groups (the correspondent momenta distributions are plotted in Figure 5.10 (a)). We obtain a p-value and a confidence level in number of σ's:

$$p_{control} = 0.527; \qquad \sigma^{KS}_{control} = 0.633 \ (\chi^2) \tag{5.29}$$

where the number of degrees of freedom is given by the number of bins in the histograms minus 1: $n.d.f. = 39$.
The correspondent p-values and confidence levels were obtained for the Kolmogorov-Smirnov (K.S.) and Anderson-Darling (A.D.) test using more finely binned histograms ($n_{bin} = 1000$), as suggested on the ROOT reference manual:

$$p^{KS}_{control} = 0.245; \qquad \sigma^{KS}_{control} = 1.16 \ (K.S.) \tag{5.30}$$

$$p^{AD}_{control} = 0.264; \qquad \sigma^{AD}_{control} = 1.12 \ (A.D.) \tag{5.31}$$

As a second control we decided to apply the test to the real momenta from the nominal and shifted samples. A fiducial cut was applied by selecting only the CC events whose vertexes were not on the outer layer of the calorimeter and for which the vertex true x coordinate was $|x_V^{truth}| < 1.5$ m (the two distributions are plotted

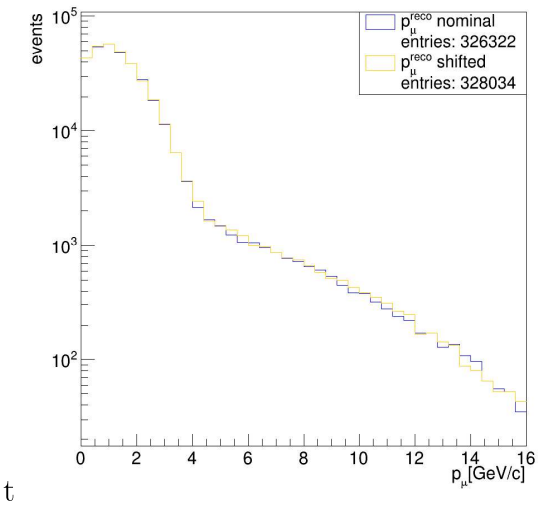

t

Figure 5.11: Reconstructed momenta distributions from the nominal and shifted samples. The fiducial and reconstruction selections are applied. Both histograms are in logarithmic scale.

in Figure 5.10 (b)). This was done in order to gauge what the best possible p-value (i.e. the smallest and most decisive) might be:

$$p_{truth} = 5.15 \times 10^{-7}; \qquad \sigma_{truth} = 5.02\ (\chi^2) \tag{5.32}$$

$$p^{KS}_{truth} = 1.41 \times 10^{-4}; \qquad \sigma^{KS}_{truth} = 3.81\ (K.S.) \tag{5.33}$$

$$p^{AD}_{truth} = 1.26 \times 10^{-4}; \qquad \sigma^{AD}_{truth} = 3.83\ (A.D.) \tag{5.34}$$

No p-value obtained from the reconstructed momenta should be smaller than p_{truth}.

5.3.3 Results

The first two samples considered for beam monitoring are the muon reconstructed momenta after the fiducial cut and the selection on the successfulness of the reconstruction are applied. The reconstructed momentum distributions of the muons produced with nominal and shifted neutrino fluxes are shown in Figure 5.11.
Applying the statistical tests on the reconstructed momenta samples we find:

$$p_{reco} = 1.55 \times 10^{-3}; \qquad \sigma_{reco} = 3.17\ (\chi^2) \tag{5.35}$$

$$p^{KS}_{reco} = 0.382; \qquad \sigma^{KS}_{reco} = 0.874\ (K.S.) \tag{5.36}$$

$$p^{AD}_{reco} = 0.158; \qquad \sigma^{AD}_{reco} = 1.41\ (A.D.) \tag{5.37}$$

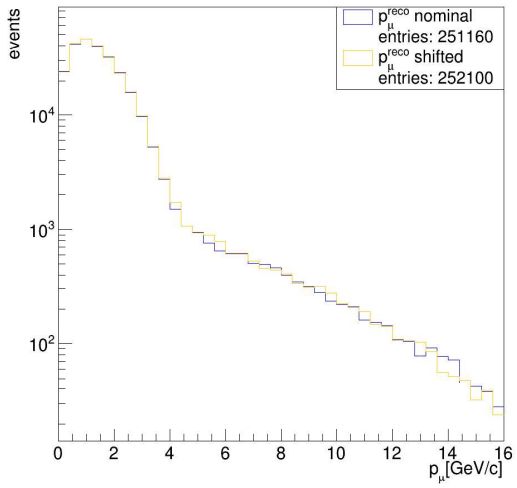

Figure 5.12: Reconstructed momenta distributions from the nominal and shifted samples. The fiducial, reconstruction and quality selections are applied. Both histograms are in logarithmic scale.

We repeat the procedure by applying the quality cut described in Section 5.2.4 to both samples (reconstructed momentum distributions for the new samples are shown in Figure 5.12). The new p-values and significance levels from the reconstructed samples are:

$$p_{reco} = 1.55 \times 10^{-4}; \qquad \sigma_{reco} = 3.78\ (\chi^2) \tag{5.38}$$

$$p_{reco}^{KS} = 0.295; \qquad \sigma_{reco}^{KS} = 1.05\ (K.S.) \tag{5.39}$$

$$p_{reco}^{AD} = 0.137; \qquad \sigma_{reco}^{AD} = 1.49\ (A.D.) \tag{5.40}$$

Evolution of p-value and sigma with the sample

In order to study how the p-value and significance level grew with the data, we applied the χ^2 to increasingly larger samples. We show the results for quality cut reconstructed momenta samples in Figure 5.13. As we should expect as the samples become larger the χ^2 and number of σ's grow, while the p-value decreases.

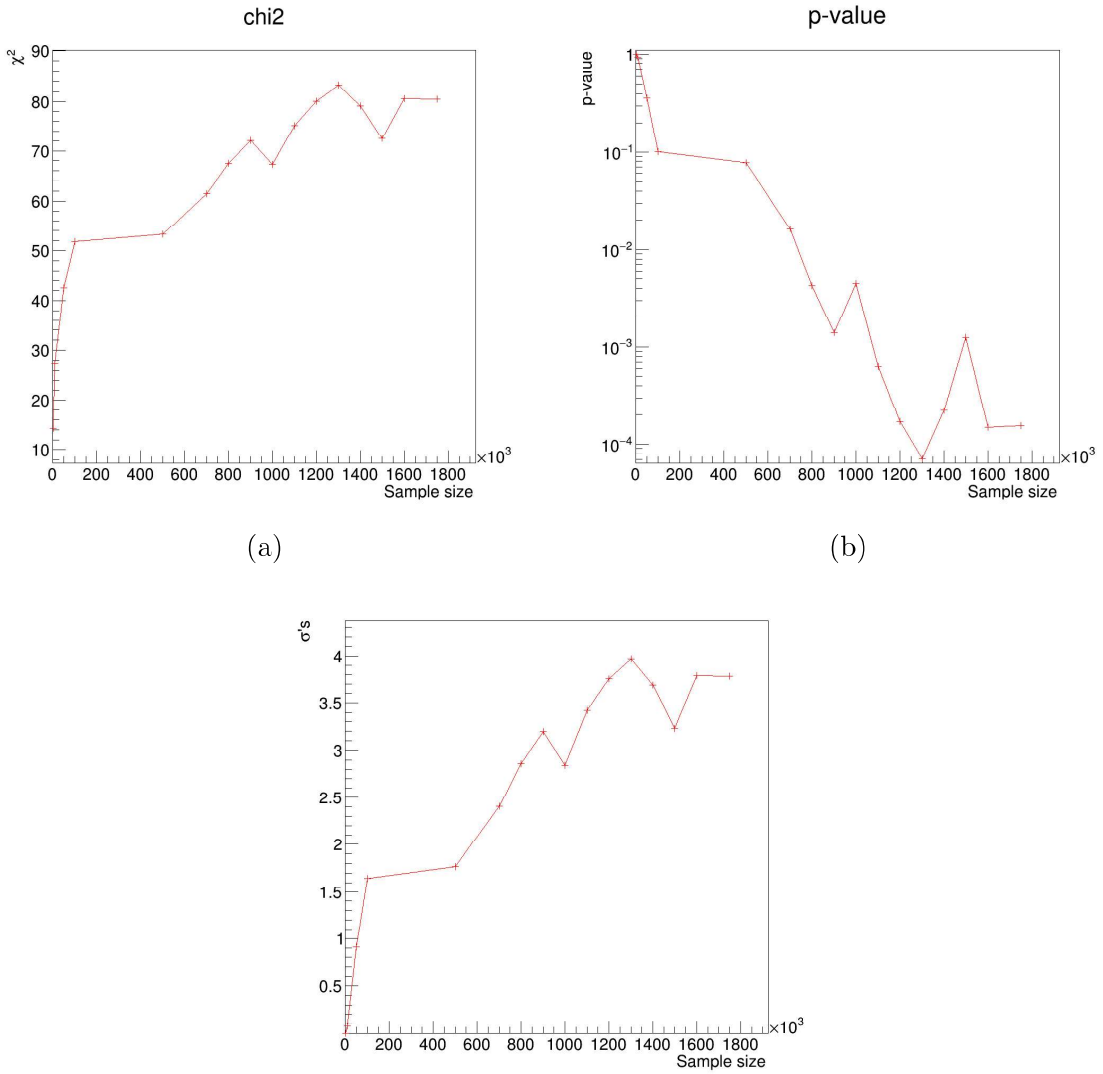

(a) (b)

(c)

Figure 5.13: Evolution of the values of (a) χ^2, (b) p-value and (c) confidence level in number of sigmas for increasingly larger samples where all the cuts were applied. On the x-axis we show the size of the total event sample before any cut was applied.

Conclusions

We used a χ^2 two-sample test to assess the capability of the SAND detector to monitor neutrino beam changes on a weekly basis. We compared the reconstructed muon momentum spectra generated in a week by CC ν_μ interactions produced with reference beam configuration, with the one produced on the same time span by a displacement of 0.5 mm of the second beam horn over one transversal axis.
In order to meet the weekly requirement, we used the front part of the SAND barrel calorimeters as neutrino target to provide enough mass. We then produced the two datasets using a detailed simulation, which starts from the beam energy spectrum, simulates neutrino interactions, propagates their products inside SAND and digitizes the response of the crossed detectors. Generated events were then reconstructed and analysed using custom made software based on standard techniques.
Considering a 0.5 mm horn displacement we observe that even in the case of a perfect detector with a perfect reconstruction, (i.e. using the Monte Carlo "truth"), the significance of the difference among the two datasets does not exceed 5 σ, thus defining our sensitivity limit.
After a detailed analysis, we found that we are able to separate the two reconstructed samples at 3.8 σ confidence level, a significant result, in view of the considerations expressed above.
This result, although already within the DUNE requirements, can still be improved, for instance, by also including in the dataset the events with a neutrino interaction in the STT, not considered in this study. In this case, while the "true" sample will marginally increase its sensitivity due to the larger statistics, we expect that the improved resolution on the reconstructed quantities, due to the lack of multiple scattering in the calorimeter, will be useful to get the discriminating power of the reconstructed samples closer to the ideal one.
Another promising route would be to consider the reconstructed position on the xy plane of the interaction vertexes, either in the front calorimeters or in the STT. We expect that a modification in the beam production would produce a change both in the median of the transverse space distribution and on its shape. Unfortunately the flux spectra used to simulate the neutrino interactions for this thesis contained no spatial informations, making it impossible to consider the vertex position distribution in the study. Detailed simulations of the neutrino production kinematics produced by the Fermilab accelerator group are currently being validated and will soon be available, allowing to explore this hypothesis.